

Synthesis, Structural, Electrical, Magnetic Curie Temperature and Y–K Angle Studies of Mn–Cu–Ni Mixed Spinel Nanoferrites

Ahmad Faraz · Asghari Maqsood

Received: 20 July 2011 / Accepted: 20 September 2011 / Published online: 11 November 2011
© Springer Science+Business Media, LLC 2011

Abstract Nanoferrites of composition $\text{Mn}_{0.50}\text{Cu}_{0.5-x}\text{Ni}_x\text{Fe}_2\text{O}_4$ ($0.00 \leq x \leq 0.50$) are prepared by chemical coprecipitation method. The prepared nano-ferrites were characterized by X-ray diffraction (XRD), scanning electron microscopy (SEM), infrared spectroscopy (IR), two probe resistivity apparatus, and vibrating sample magnetometer (VSM) to study the compositional, structural, morphological, electrical, and magnetic properties with varying concentration (x) in the composition of the prepared nanoferrites. XRD confirmed formation of single phase spinel ferrite with crystalline size in the range of 16–29 nm. The lattice parameter (a) decreases with a decrease of Cu concentration. Further information about the structure and morphology of the nanoferrites was obtained from SEM and results are in good agreement with XRD. FTIR gives information about distribution of cations and anions by confirming the presence of high and low frequency bands due to tetrahedral and octahedral sites, respectively. The electric properties were measured and analyzed by using homemade two probe resistivity apparatus showing semiconducting behavior of synthesized ferrites. The magnetic hysteresis curves clearly indicate the soft nature of the prepared samples. Various magnetic parameters such as saturation magnetization (M_s), and remanence (M_r) are calculated from the hysteresis loops and observed compositional dependent. Saturation magnetization and magnetic moment increase with Ni content. This is due to the existence of localized canted spin. Coercivity and

M_s decreases while Y–K angles increase with Cu^{2+} content. The Ni^{2+} addition improves the magnetic properties. Curie temperature decreases with increase in Cu contents.

Keywords Coercivity · $\text{Mn}_{0.50}\text{Cu}_{0.5-x}\text{Ni}_x\text{Fe}_2\text{O}_4$ · Saturation magnetization · Spinel nanoferrites · Nanostructure · Remanence · Curie temperature

1 Introduction

Ferrites have a wide range of applications from microwave to radio frequencies, exhibiting very low conductivity, which is an important requirement for microwave applications. In the spinel type structure, cations and anions are distributed between two different sites: tetrahedral (A) and octahedral (B) sites. Magnetic as well as electrical properties of these ferrites strongly depend on the distribution of cations at the different sites as well as the preparation method and conditions [1]. Ferrite nanoparticles have been synthesized by using a number of techniques such as sol-gel autocombustion method, refluxing method, mechanical grinding, and hydrothermal methods, etc. [2–5]. For the preparation of ferrites, chemical coprecipitation method has been widely used. Among these, the chemical coprecipitation technique is economical and easy to utilize. Soft magnetic ferrites are important technological materials because they have high resistivity, high mechanical strength, high Curie temperature, magneto-optic, and corrosion resistant properties [6]. Ferrites have high resistivity and permeability. In ferrites, cations occupied two types of positions sites (e.g., octahedral (A) and tetrahedral (B) sites). However, properties of ferrites may be influenced by several other factors, including covalent bonding effect and crystal field stabilization energies of transition-metal cations. The presence of cations in the interstitial sites distorts the oxygen

A. Faraz (✉) · A. Maqsood
Thermal Transport Laboratory, School of Chemical and Materials Engineering, National University of Sciences and Technology (NUST), NUST H-12 Campus, Islamabad 44000, Pakistan
e-mail: faraz.nust83@gmail.com

A. Maqsood
e-mail: tpl.qau@usa.net

sublattice and the tetrahedrally coordinated sites to be expanded, effecting a light displacement of the oxygen anions along the cell diagonals. Among the transition-metal series, the d-electron structure of the cations changes in systematic way, whereas the ionic radius relatively remains constant. This leads to an excellent opportunity to engineer and fabricate specific magnetic interactions in the crystal lattice by substituting various transition-metal cations in the crystal structure, thereby altering macroscopic and microscopic magnetic properties [7]. MnFe_2O_4 has a normal-type spinel structure. Contrary to MnFe_2O_4 , Ni ferrite typically have an inverse-spinel structure, where Ni ions prefer to occupy B site. It is ferrimagnetic material belonging to a group of soft ferrite materials, having a typical spin arrangement of $[\text{Fe}^{3+}(\uparrow)]^A[\text{Ni}^{2+}(\uparrow)^-, \text{Fe}^{3+}(\uparrow)]^B\text{O}_4$. Ferrites having Ni as constituent exhibit excellent magnetic and electronic properties [8]. On the basis of these properties, we have synthesized complex spinel Nanoferrites of $\text{Mn}_{0.5}\text{Cu}_{0.5-x}\text{Ni}_x\text{Fe}_2\text{O}_4$ with systematic variation of concentration x by chemical coprecipitation method. The prepared nanoferrites are characterized and studied by X rays diffraction (XRD), infrared spectroscopy (IR), scanning electron microscopy (SEM), two probe resistivity apparatus, and vibrating sample magnetometer (VSM) to investigate the compositional, structural, morphological electrical and magnetic properties.

2 Experimental

2.1 Synthesis

Various preparation techniques have been employed for the synthesis of ultrafine nanoparticles of ferrites, which exhibit novel properties. Various techniques includes sol–gel, coprecipitation, thermal decomposition, and hydrothermal methods. Ultrafine homogenous nanoferrite particles can be prepared by the simple chemical coprecipitation method. Control of particle size in the nanometer is difficult task because of variation of dopant concentration can affect particle size. It becomes mandatory in the case of ferrofluid preparation using the coprecipitation method. In case of ferrofluid, it is mandatory that the synthesized sample is prepared with the help of the coprecipitation method [9]. Chemical precipitation is the economical route for the production of large scale of ultrafine nanoferrite particles [10]. Among different methods, the preparation of nanoferrites by the chemical coprecipitation method provides many advantages due to its relative simple reaction procedure, homogenous mixing, lesser cost, and good control over the particle size and structure [11, 12]. In this paper, a series $\text{Mn}_{0.5}\text{Cu}_{0.5-x}\text{Ni}_x\text{Fe}_2\text{O}_4$ ($0.00 \leq x \leq 0.50$) are prepared using chemical coprecipitation method. All used chemicals used were analytical graded and used without further purification. Procedure involves the preparation of aqueous solutions of

Ni $(\text{NO}_3)_2 \cdot 6\text{H}_2\text{O}$, Mn $(\text{NO}_3)_2 \cdot 4\text{H}_2\text{O}$, Cu $(\text{NO}_3)_2 \cdot 1/2\text{H}_2\text{O}$, and Fe $(\text{NO}_3)_3 \cdot 9\text{H}_2\text{O}$ in an alkaline medium of NaOH. NaOH with 3 M concentration was used as the coprecipitation agent. Separate solutions of Ni $(\text{NO}_3)_2 \cdot 6\text{H}_2\text{O}$, Mn $(\text{NO}_3)_2 \cdot 4\text{H}_2\text{O}$ and Cu $(\text{NO}_3)_2 \cdot 1/2\text{H}_2\text{O}$ (with a total concentration of 0.1 M), and Fe $(\text{NO}_3)_3 \cdot 9\text{H}_2\text{O}$ (0.2M) were prepared in 100 ml of deionized water. An example to prepare ferrites with the composition of $\text{Mn}_{0.5}\text{Cu}_{0.4}\text{Ni}_{0.1}\text{Fe}_2\text{O}_4$ (with $x = 0.10$) is described as. For this composition, the stoichiometric reagent ratio of 0.05 M of Mn $(\text{NO}_3)_2 \cdot 4\text{H}_2\text{O}$, 0.04 M of Cu $(\text{NO}_3)_2 \cdot 1/2\text{H}_2\text{O}$ and 0.01 M of Ni $(\text{NO}_3)_2 \cdot 6\text{H}_2\text{O}$ and 0.2 M of Fe $(\text{NO}_3)_3 \cdot 9\text{H}_2\text{O}$ were used. These reagents were taken separately in 100 ml deionized water followed by mixing the prepared solutions in a beaker; at 85 °C with constant magnetic stirring until a clear solution was obtained. Solution of coprecipitating agent of NaOH (3 M) was made separately in 100 ml of deionized water and heated up to 85 °C. The solution of coprecipitating agent then mixed rapidly with the prepared salt solutions. It is important to mention here that rapid mixing of metal solution with coprecipitating agent gives relatively small size homogenous nanoparticles. For transforming metallic hydroxide into ferrites, the temperature was increased to make a reaction fast; the temperature was kept constant at available 310 °C. After mixing a metallic solution with NaOH solution, both solutions were heated and stirred for 40 minutes. This was followed by stoppage of heating while constant stirring remained and continued for 3 hours. The pH value was kept between 11.25 and 12.35. Precipitates were washed 5 times with de ionized water. Products were dried with the help of electric oven over night at 110 °C. At the end, a black colored ferrite powder was obtained. Similarly, all six types of compositions were synthesized by varying the desired stoichiometric amounts of salts. Dried samples were sintered in a furnace for about six hours at 800 °C. This was followed by cooling of the furnace at 10 °C/min.

2.2 Analysis and Characterization

The prepared $\text{Mn}_{0.5}\text{Cu}_{0.5-x}\text{Cu}_x\text{Fe}_2\text{O}_4$ ($0.00 \leq x \leq 0.50$) ferrites were characterized by various techniques. Structural and related characteristics of the samples were determined by X-ray diffraction (XRD) using a Stoe diffractometer to determine the lattice parameter, phases, particle size, and X-rays density, etc. XRD patterns were obtained using Cu $K\alpha$ ($\lambda = 1.5406 \text{ \AA}$) at room temperature. The mean crystallite sizes were estimated using the standard Scherrer formula. Furthermore, analysis was then performed on the XRD data to obtain the lattice constants, crystallite size, lattice constant, a , and XRD density ρ_x using the standard relations as described elsewhere [6]. Compositional analyses were performed using XRF (JEOL JAPAN JSX3201M). Transmission IR spectra were obtained by Perkin Elmer FTIR

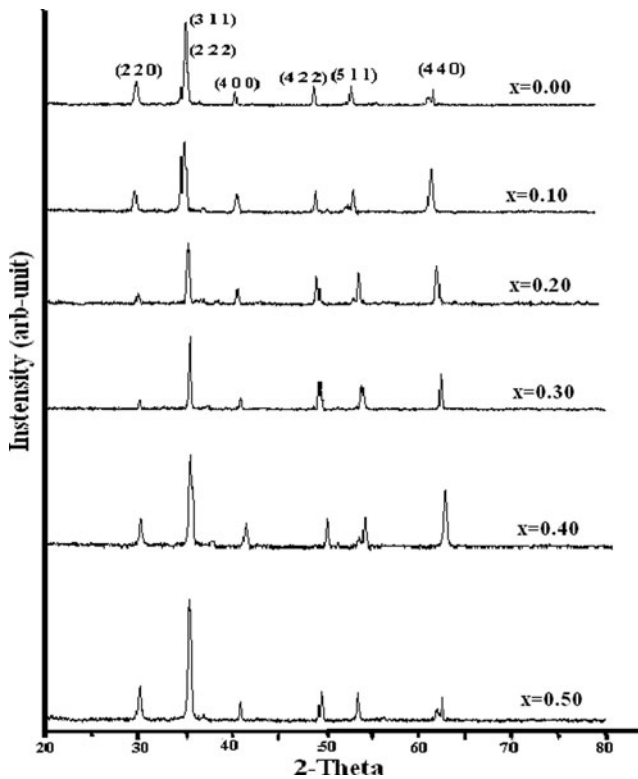


Fig. 1 The XRD patterns of $\text{Mn}_{0.5}\text{Cu}_{0.5-x}\text{Ni}_x\text{Fe}_2\text{O}_4$ nanoferrites with varying concentrations (x)

spectrometer using KBr and synthesized samples disc pellet. Morphology and structure of the nanoferrites were studied using scanning electron microscopy (SEM), Jeol JSM 6490A. Since due to high resistivity of synthesized material, SEM could not be performed on the samples fabricated discs. To overcome this problem, circular discs were made conducting with gold coating. Electrical, magnetic, and Curie temperature measurements were done using a vibrating sample magnetometer (VSM) model, BHV 50, Riken Denshi Co. Ltd. Japan, Laboratory resistivity and susceptibility apparatus.

3 Results and Discussion

3.1 Structural and Morphological Studies

The indexed XRD patterns of the prepared samples of $\text{Mn}_{0.5}\text{Cu}_{0.5-x}\text{Ni}_x\text{Fe}_2\text{O}_4$ are presented in Fig. 1. The presence of planes (220), (311), (222), (400), (422), (440), and (511) in the diffractograms confirmed the cubic spinel structure. As it is evident from the figure that $\text{Mn}_{0.5}\text{Cu}_{0.5-x}\text{Ni}_x\text{Fe}_2\text{O}_4$ with varying compositions exhibit single phase spinel structure without showing any other detectable impurity. The peaks broadening indicate lower crystallite size of the synthesized samples. The average crystallite size for each

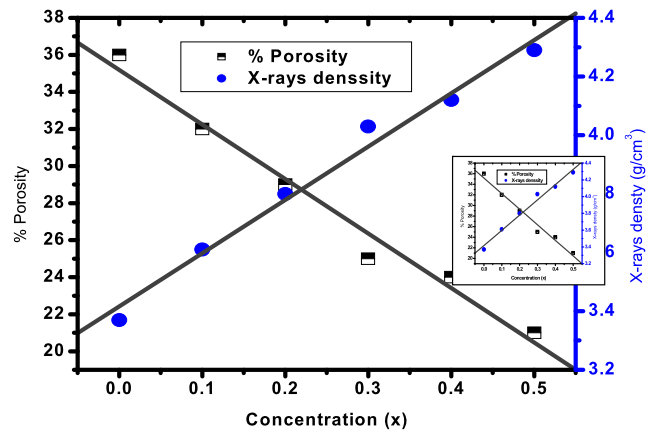
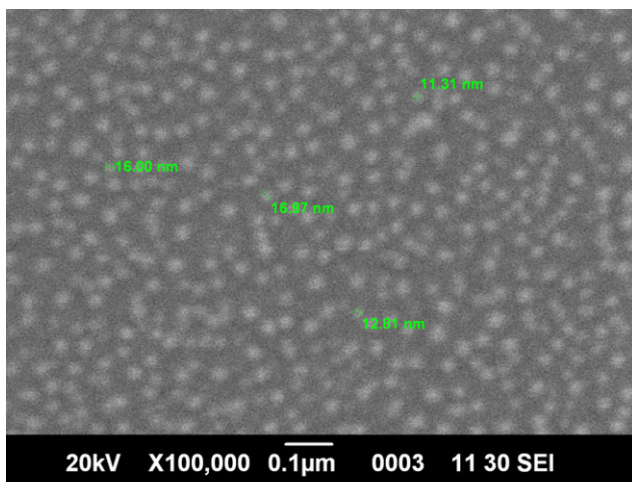
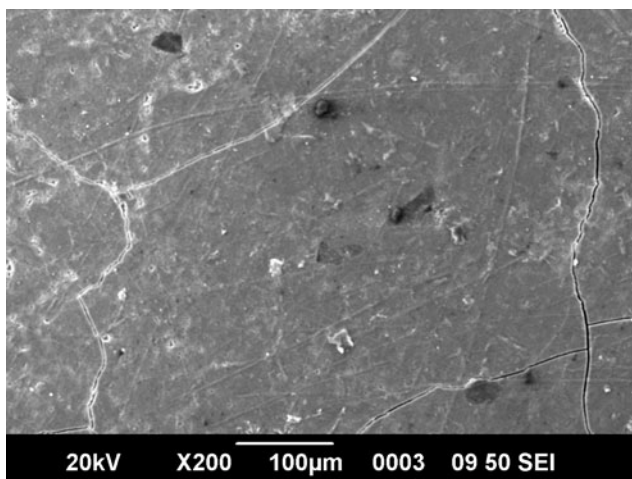


Fig. 2 Variation in the porosity (P) and X-ray density (ρ_x). Inset graph shows relation between porosity and measured density of $\text{Mn}_{0.5}\text{Cu}_{0.5-x}\text{Ni}_x\text{Fe}_2\text{O}_4$

composition was calculated using the standard Scherrer formula the XRD peak corresponding to the total average peaks of the planes of the spinel structure [13]. The crystallite size remained within the range 16–9 nm. XRD data was also used to calculate various characteristics of the prepared nano-ferrites such as lattice constant (a), average crystallite size (t (ave)), volume of the cell (V), X ray density (ρ_x), and porosity (P) using standard relationships as discussed elsewhere [14]. It is observed that the lattice constant decreases with the increase Ni concentration. This may be due to the difference in ionic radius of the copper ions (0.73 Å) and Ni (0.69 Å). Addition of copper at the expense of Ni in the ferrite is expected to increase the lattice constant. Figure 2 determines a variation in porosity and X-rays density and the inset graph shows variation in porosity and measured density with concentration and values tabulated in Table 1. It is observed that porosity decreased as the concentration Cu concentration decreased; again it is due to the difference in ionic radius of Cu and Ni. The measured (ρ_m) and X-rays density (ρ_x) of the corresponding materials are found in range from 5.24 to 5.4 g/cm^3 and 3.37–4.29 g/cm^3 . Morphological analyses was done with help of scanning electron microscopy (SEM). SEM micrographs of prepared $\text{Mn}_{0.5}\text{Cu}_{0.5-x}\text{Ni}_x\text{Fe}_2\text{O}_4$ ($x = 0.0$) nanoferrites are shown in Fig. 3(a, b). As seen from the micrographs 3(a), at high resolutions, determines the dimension of the particle is varying in the range of 16–21 nm. Figure 3b at a lower resolution shows the surface morphology of the sample $\text{Mn}_{0.5}\text{Cu}_{0.5-x}\text{Ni}_x\text{Fe}_2\text{O}_4$ with x (0.00), respectively. Relatively porous, dense material formation is apparent in the samples with a remarkable change in grain size. The average grain size determined by the SEM for sample $\text{Mn}_{0.5}\text{Cu}_{0.5-x}\text{Ni}_x\text{Fe}_2\text{O}_4$ $x = 0.00$ is fairly consistent with that obtained from the XRD technique. The comparison of the results of XRD (Table 1) and SEM reveals that the substitution of Ni ions for Cu in the $\text{Mn}_{0.5}\text{Cu}_{0.5-x}\text{Ni}_x\text{Fe}_2\text{O}_4$



(a)



(b)

Fig. 3 Scanning electron microscopy (SEM) of the nanoferrites of $\text{Mn}_{0.5}\text{Cu}_{0.5-x}\text{Ni}_x\text{Fe}_2\text{O}_4$ with concentration of $x = 0.00$ (a) low resolution; (b) high resolution

ferrite system shows an increase in bulk density and decrease in porosity and particle size of the host material. Similar to these observations are reported in [15].

3.2 Infrared Spectroscopy Studies

IR-spectroscopy reveals the distribution of cations and anions on octahedral and tetrahedral sites. In the current work, IR spectra of Mn-Cu-Ni ferrites were examined in the frequency range of $350\text{--}1000\text{ cm}^{-1}$. Figure 4 represent IR spectrums of the prepared ferrites of $\text{Mn}_{0.5}\text{Cu}_{0.5-x}\text{Ni}_x\text{Fe}_2\text{O}_4$. Two main metal–oxygen bands, e.g., higher and lower frequency bands are important in ferrites to determine octahedral and tetrahedral cations and anions positions [16]. In Fig. 4 IR band, ν_1 , is usually observed in the higher frequency range of $620\text{--}550\text{ cm}^{-1}$. The ν_1 band corresponds to internal stretching vibrations of the

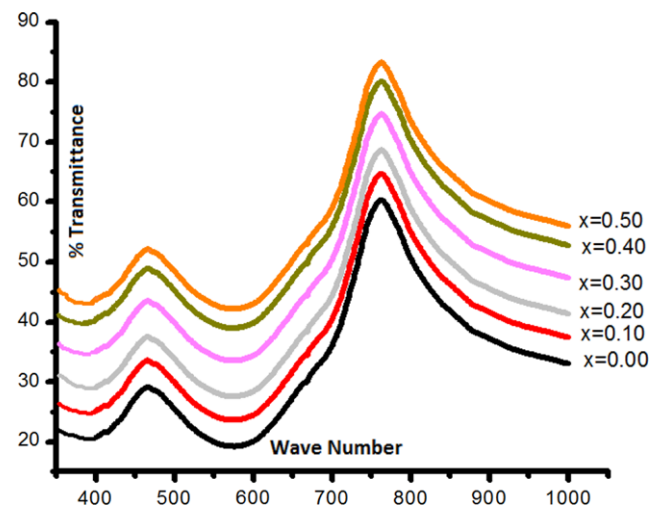


Fig. 4 FTIR-spectra of the prepared $\text{Mn}_{0.5}\text{Cu}_{0.5-x}\text{Ni}_x\text{Fe}_2\text{O}_4$ nanoferrites of with varying concentrations (x). ν_1 and ν_2 designate high and low energy frequency bands, respectively

metal atoms at the tetrahedral site, $M_{\text{tetra} \leftrightarrow \text{O}}$. The second band is ν_2 , a lowest frequency band which is observed in the range of $360\text{--}425\text{ cm}^{-1}$. This is assigned to the octahedral metal atoms vibrational stretching, $M_{\text{octa} \leftrightarrow \text{O}}$.

3.3 Electrical Properties

The electrical resistivity is important properties of ferrites, particularly for high-frequency applications. The resistivity of the ferrites depends on several factors such as density, porosity, grain size, chemical composition, etc. In the current paper, dc electrical resistivity was determined by a Laboratory two-probe method in the temperature range $375\text{--}575\text{ K}$. Arrhenius relation (1) was used to obtain dc electrical resistivity (ρ_{dc}) at specific temperatures. From the slope of the Arrhenius plot, activation energy was determined [17]:

$$\rho_T = \rho_o \exp\left(\frac{\Delta E}{k_B T}\right) \quad (1)$$

where ΔE is the activation energy in (eV), k_B is the Boltzmann constant, and T is the temperature in Kelvin (K). The values of activation energy are tabulated in Table 1. In Fig. 5, the variation of dc electrical resistivity of $\text{Mn}_{0.5}\text{Cu}_{0.5-x}\text{Ni}_x\text{Fe}_2\text{O}_4$ ($0.00 \leq x \leq 0.50$) as a function of temperature is shown. The DC resistivity was found for all samples and was found in the range of $2.2 \times 10^6\text{--}5 \times 10^6\ \Omega\text{-cm}$ as illustrated in Table 1. From the inset in Fig. 5, it is clear that resistivity decreases with an increase in temperature for all the synthesized samples confirmed with semiconducting behavior. The conduction mechanism in ferrites can be explained by a hopping mechanism [18, 19]. The activation energy was determined from the slope of the $\ln \rho$ versus $(1/k_B T)$. The activation energy (ΔE) of the studied specimens was found in the range $0.16\text{--}0.25$ (eV) with

Table 1 The average crystallite size (t (ave)), lattice constant (a), lattice volume (V), measure density (ρ_m), X-rays density (ρ_x), porosity (P), dc electrical resistivity (ρ_{dc}), activation energy (ΔE), correlation factor (R), drift mobility (μ_d), coercivity (H_c), saturation magnetization (M_s), remnant magnetization (M_r), squareness ratio (M_r/M_s), Bohr's magneton, Y-K angle (degree), Curie temperature (T_c) of the $Mn_{0.5}Cu_{0.5-x}Ni_xFe_2O_4$ ferrites with varying concentrations $0 \leq x \leq 0.5$

Parameters	Ferrites compositions					
	$Mn_{0.5}Cu_{0.5}Fe_2O_4$ X = 0.00	$Mn_{0.5}Cu_{0.4}Ni_{0.1}Fe_2O_4$ X = 0.10	$Mn_{0.5}Cu_{0.3}Ni_{0.2}Fe_2O_4$ X = 0.20	$Mn_{0.5}Cu_{0.2}Ni_{0.3}Fe_2O_4$ X = 0.30	$Mn_{0.5}Cu_{0.1}Ni_{0.4}Fe_2O_4$ X = 0.40	$Mn_{0.5}Ni_{0.5}Fe_2O_4$ X = 0.50
t_{avg} (nm)	16	17.23	19.11	22	26	29
a (Å)	8.47	8.43	8.42	8.4	8.37	8.34
V (Å) ³	607	599	596	592	586	580
ρ_m (g cm ⁻³)	5.24	5.26	5.31	5.34	5.36	5.4
ρ_x (g cm ⁻³)	3.37	3.61	3.8	4.03	4.12	4.29
P (fraction)	0.36	0.32	0.29	0.25	0.24	0.21
ρ_{dc} ($\times 10^6 \Omega\text{-cm}$) (373 K)	2.2	2.7	3.62	4.17	4.41	5
$\sqrt{\rho}$	1.48	1.64	2	2.04	2.1	2.23
ΔE (eV)	0.25	0.21	0.20	0.18	0.17	0.16
R	0.98	0.98	0.98	0.98	0.98	0.98
μ_d ($\times 10^{-11} \text{ cm}^2 / (\text{V}\cdot\text{s})$) (373 K)	16.4	13.4	10	8.68	8.21	7.24
H_c	149	192	224	296	376	525
M_s	11	12	14	15	18	21
M_r	1.6	2.1	2.32	2.81	3.1	3.37
M_r/M_s	0.13	0.17	0.15	0.18	0.17	0.15
n_B	0.16	0.14	0.12	0.11	0.097	0.091
Y-K angle	57	52	47.62	40.53	33.51	22
T_c (K)	443	490	545	597	623	715

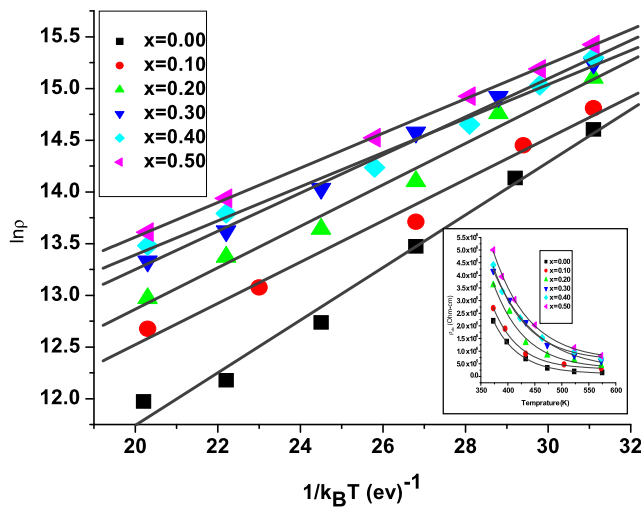


Fig. 5 Resistivity as a function of temperature at various concentrations X . *Inset* graph shows dependence of temperature on the electrical resistivity for the nanoferrites of $\text{Mn}_{0.5}\text{Cu}_{0.5-x}\text{Ni}_x\text{Fe}_2\text{O}_4$ ($0.00 \leq x \leq 0.50$). Straight lines are the best fit to (1)

a maximum value for $x = 0.00$. The activation energy values are in good agreement with previously reported values for other spinel ferrites [19]. The drift mobility (μ_d) was determined using equation [20]:

$$\mu_d = \left(\frac{1}{ne\rho} \right) \quad (2)$$

where ρ is the resistivity, e is the electron charge, and n is the charge concentration carrier which can be calculated from the relation [21]

$$n = \left(\frac{N_A \rho_m P_{\text{Fe}}}{M} \right) \quad (3)$$

where N_A , ρ_m , and M are the Avogadro's number, measured density, and molecular weight of the corresponding sample, respectively, and P_{Fe} is the number of iron atoms in the formula $\text{Mn}_{0.5}\text{Cu}_{0.5-x}\text{Ni}_x\text{Fe}_2\text{O}_4$. The drift mobility for all the samples was calculated using (2) and (3). The plots of (μ_d) with $1/k_B T$ are shown in Fig. 6. The temperature variation of resistivity was mainly attributed due to change of drift mobility with temperature. It is observed from the graph that by increasing the temperature, the drift mobility also increases. It may be due to the fact that the charge carriers start hopping from one site to another as the temperature increases [22]. It is observed from Fig. 6 that with increasing the temperature, the drift mobility increases. It may be due to the charge carrier's start hopping from one site to another as the temperature gets increased. dc resistivity and activation energy as function of Nickel concentration are shown in Fig. 7

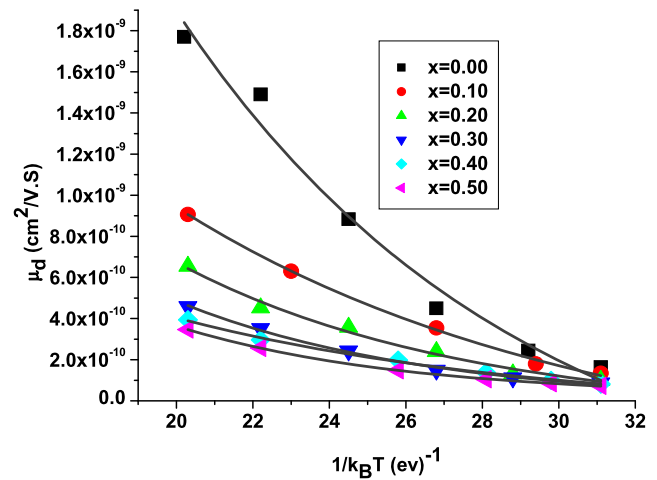


Fig. 6 Drift mobility (μ_d) as a function of temperature

3.4 Magnetic Properties

Figure 8a illustrates the variation of magnetization M (emu/g) versus the applied magnetic field H (Oe) at room temperature for the prepared $\text{Mn}_{0.5}\text{Cu}_{0.5-x}\text{Ni}_x\text{Fe}_2\text{O}_4$ spinel nanoferrites. A hysteresis loop was obtained using the vibrating sample magnetometer (VSM). The narrow loops determine the soft nature of the prepared nanoferrites. All the observed curves behave normally, and the magnetization was found to increase with an increase in the applied magnetic field and attains its maximum value for an applied field of 1.25 Tesla. Various magnetic parameters such as saturation magnetization (M_s), remanence (M_r), and coercivity (H_c) were calculated from the hysteresis loop. The values of all of these calculated parameters are given in Table 1. The dependence of M_s and coercivity (H_c) on concentration (X) is illustrated in Fig. 8b. It is observed that M_s and H_c increases with concentration (X). Coercivity represents the strength of the magnetic field necessary to surpass the anisotropic barrier and allows the magnetization of the nanomagnetic particles. Temperature influences the coercivity H_c as it has been observed in superparamagnetic specimens, and with an increase in temperature the coercivity tends to vanish with increase [23]. The obtained M_s and H_c values in the present study are found to be in the range 11–21 emu/g and 149–525 Oe. The effect of concentration on saturation magnetization (M_r) and Bohr's magneton (n_B) is shown in Fig. 8c and values are illustrated in Table 1. M_r increases with an increase in concentration (X). M_r starts to increase from 1.6 emu/g to 3.37 emu/g, respectively, as the Cu concentration is decreased. The increase in the M_s and M_r values with a decrease in Cu concentration can be explained on the basis of Neel's theory. Bohr magneton values

Fig. 7 Effect of concentrations (x) on the dc electric resistivity (ρ_{dc}) and activation energy (ΔE) of $Mn_{0.5}Cu_{0.5-x}Ni_xFe_2O_4$ nanoferrites

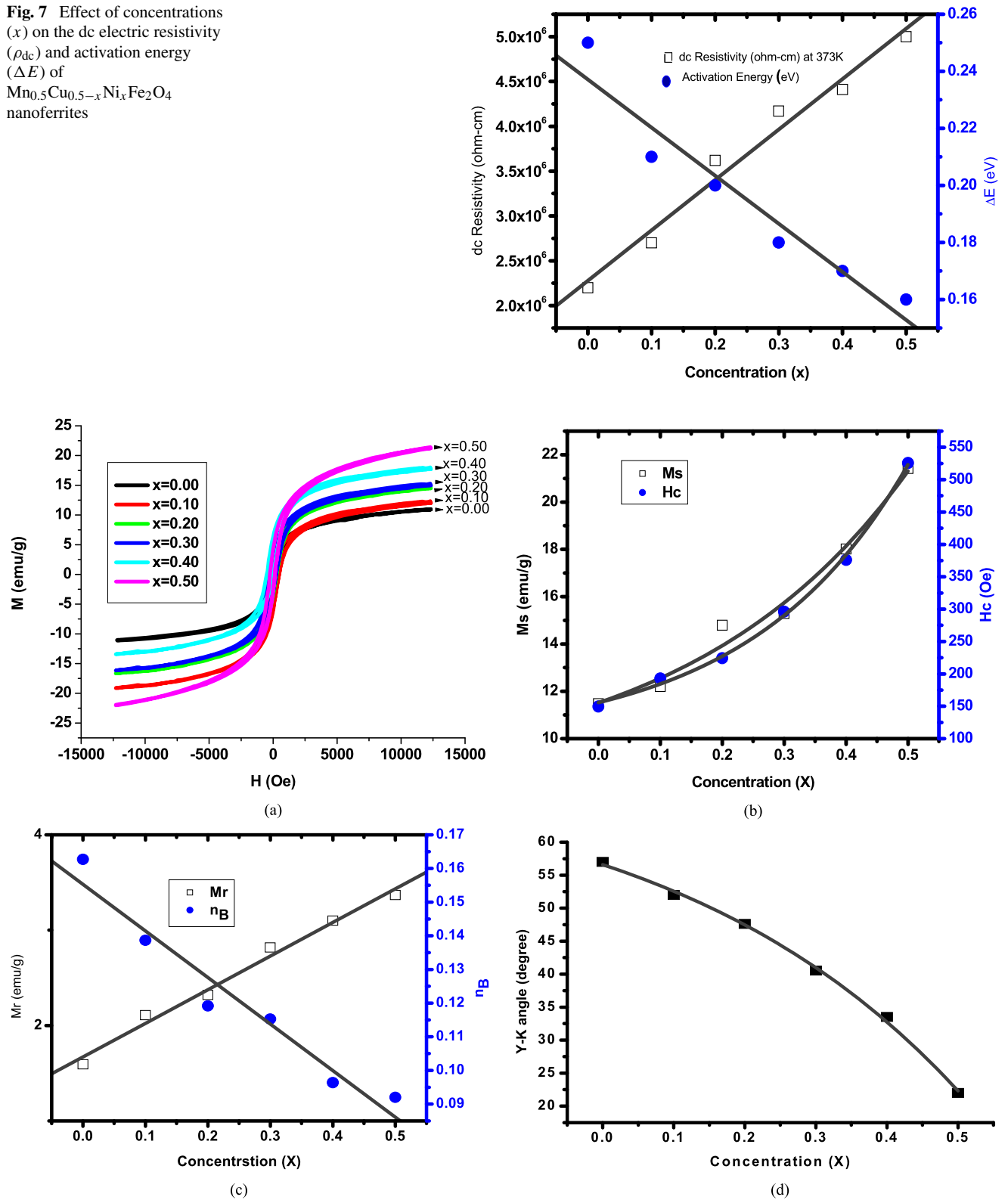


Fig. 8 Magnetic hysteresis curve of $Mn_{0.5}Cu_{0.5-x}Ni_xFe_2O_4$ for $0 \leq x \leq 0.5$ (a); saturation magnetization (M_s) and coercivity (H_c) vs. concentration (b); M_r and n_B vs concentration (c); Y-K angle vs. concentration (d)

were determined by using relation [24]. The Bohr magneton (n_B) was calculated using relation

$$n_B = \frac{M.W \times M_s}{5585 \times \rho_m} \quad (4)$$

Whereas $M.W$, M_s , and ρ_m are the magnetic moment, molecular weight, saturation magnetization, and measured density. The Bohr magneton values are illustrated in Table 1. The results obtained are in agreement with previous studies of ferrites containing Mn, Cu, or Ni ions [24–30]. In calculating the magnetic moment (n_B), we have to consider A–B interaction and cation distribution. It is observed that due to the substitution of Ni^{2+} ions at tetrahedral (A) and octahedral [B] sites in place of Cu^{2+} ions, the magnetic moment of octahedral B-site increases. It is observed that the magnetic moment decreases with an increase in Cu^{2+} . This is in agreement with the observation in [24]. The Yafet–Kittel (Y–K) angles have been calculated using the formula [31]:

$$n_B = (6 + x) \cos \alpha_{Y-K} - 5(1 - x) \quad (5)$$

where x represents concentration. The values of Y–K angles are illustrated in Table 1 and the effect of concentration on the Y–K angle at room temperature is represented in Fig. 8d. It increases exponentially with the decrease with concentration (x). The nonzero Y–K angles suggest that the magnetization behavior cannot be explained on the basis of Neel two sublattice models due to the presence of spin canting on B sites, which increases the B–B interaction, and consequently decreases the A–B interaction. These results are also in good agreement with the observation of A–B interaction in the two sub-lattices due to Ni substitution in mixed Mn ferrites by others [32]. This shows that in the present system of ferrites, randomness increases as Ni is substituted in these Cu ferrites and shows a significant departure from the Neel collinear model.

In Fig. 9, variation of Curie temperature with concentration (X) is shown. It is observed that with an increase in concentration of the Cu, the Curie temperature decreases. T_c is maximum for $\text{Mn}_{0.5}\text{Ni}_x\text{Fe}_2\text{O}_4$ while it is minimum for $\text{Mn}_{0.5}\text{Cu}_{0.5}\text{Fe}_2\text{O}_4$. The lowering of T_c can be correlated with values of Y–K angles especially in ferrites. An increase in the Y–K angle is characterized by a decrease in A–B interaction and this leads to lower the T_c in ferrites. The values of T_c are tabulated in Table 1 which are in agreement with the observation in [24, 32].

4 Conclusions

The coprecipitation method was used for the synthesis of nanoferrites of $\text{Mn}_{0.5}\text{Mg}_{0.5-x}\text{Ni}_x\text{Fe}_2\text{O}_4$ with a concentration $0.00 \leq x \leq 0.50$. Various characterizations have been

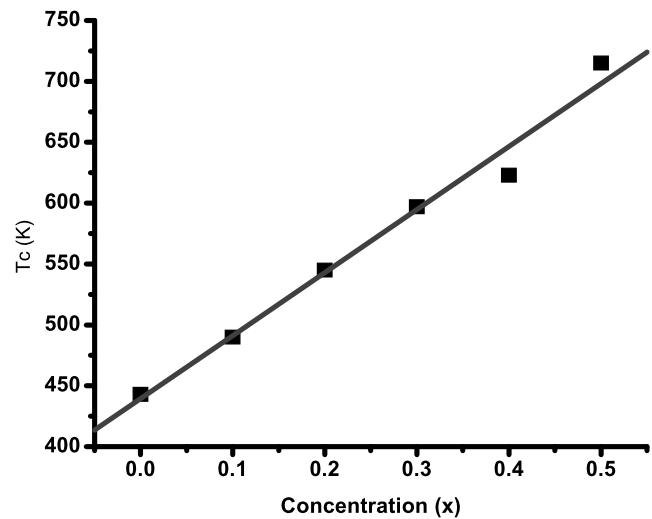


Fig. 9 Effect of concentration (X) on Curie temperature (T_c)

done to study the various electrical and magnetic properties of the synthesized nanoferrites. XRD confirmed the formation of a single phase spinel Mn–Mg–Ni ferrite structure with the size of the nanoferrites in the range of 16–29 nm and the result is in agreement with SEM results. The lattice constant and porosity were found to decrease with a decrease in the Cu contents. These observations are attributed due to the relative larger ionic radii of Cu^{2+} as compared to Ni^{2+} . The observed results suggest that the structure, composition, and morphology of the synthesized nanoferrites can be controlled by varying the composition of Mn–Cu–Ni ferrites $\text{Mn}_{0.5}\text{Cu}_{0.5-x}\text{Ni}_x\text{Fe}_2\text{O}_4$. Higher and lower frequency bands attribute to positions of cations, e.g., tetrahedral and octahedral sites of the prepared spinel-ferrites were observed using FTIR spectroscopy. A slight variation in the bands is attributed to the relative size variation between Cu and Ni metal ions. Furthermore, the hysteresis loop indicates the soft nature of the prepared nanoferrites. Saturation magnetization (M_s), remanence (M_r), H_c , and Bohr magneton (n_B) are calculated from the hysteresis loop and found to increase with Ni concentration (X) in the prepared nanoferrites. The Y–K angle strongly varies with composition and affects the Curie temperature of the synthesized material.

Acknowledgements Authors acknowledge the Pakistan Science Foundation (PSF) for financial support through Project No. 147.

References

1. Mansour, S.F.: J. Magn. Magn. Mater. **323**, 1735–1740 (2011)
2. Srivastava, P., Kapoor, I.P.S., Singh, G.: J. Alloys Compd. **485**, 88–92 (2009)
3. Pankov, V.V., Pernet, M., Germi, P., Mollard, P.: J. Magn. Magn. Mater. **120**, 69 (1993)
4. Kumar, P.S.A., Shrotri, J.J., Deshpande, C.E.: J. Appl. Phys. **81**, 4788 (1997)

5. Dias, A., Moreira, R.L., Mohallen, N.D.S.: *J. Magn. Magn. Mater.* **172**, L9–L14 (1997)
6. Javed, T., Maqsood, A.: *J. Supercond. Nov. Magn.* (2011). doi:10.1007/s10948-011-1168-7
7. Shokrollahi, H., Janghorban, K.: *Mater. Sci. Eng. B, Solid-State Mater. Adv. Technol.* **141**, 91–107 (2007)
8. Saito, F., Toyoda, T., Mori, T., Tanaka, M., Hirano, K., Sasaki, S.: *J. Phys. B, At. Mol. Phys.* **270**, 35–44 (1999)
9. Arulmurugana, R., Jeyadevanb, B., Vaidyanathana, G., Sendhilnathan, S.: *J. Magn. Magn. Mater.* **288**, 470–477 (2005)
10. Dey, S., Ghose, J.: *Mater. Res. Bull.* **38**, 1653 (2003)
11. Apesteguy, J.C., Jacobo, S.E., Schegoleva, N.N., Kurlyandskaya, G.V.: *J. Alloys Compd.* **495**, 509–512 (2010)
12. K Sharma, R., Suwalka, O., Lakshmi, N., Venugopalan, K., Banerjee, A., Joy, P.A.: *Mater. Lett.* **59**, 3402–3405 (2005)
13. Devan, R.S., Kolekar, Y.D., Chougule, B.K.: *J. Phys., Condens. Matter* **18**, 9809–9821 (2006)
14. Maqsood, A., Khan, K., Anis-ur-Rehman, M., Malik, M.A.: *J. Supercond. Nov. Magn.* **24**, 617–622 (2011)
15. Naem, M., Shah, N.A., Gul, I.H., Maqsood, A.: *J. Alloys Compd.* **487**, 739–743 (2009)
16. Brabers, V.A.M.: *Phys. Status Solidi* **33**, 563 (1969)
17. Smit, J., Wijn, H.P.J.: *Ferrites*, p. 233. Wiley, New York (1959)
18. Verwey, E.J.W., Boer, F.De., Vsanten, H.H.: *J. Chem. Phys.* **161**, 1091 (1948)
19. Sayed, E.A.M.: *Mater. Chem. Phys.* **82**, 583 (2003)
20. Mott, N.F., Davis, E.A.: *Electronic Proc. in Non-Cryst. Mat.* Oxford, London (1979)
21. Iwauuchi, K.: *Jpn. J. Appl. Phys.* **10**, 1520 (1971)
22. Austin, I.G., Mott, N.F.: *Adv. Phys.* **18**, 41 (1969)
23. Kavas, H., Baykalb, A., Toprakc, M.S., Koseoglua, Y., Sertkol, M., Aktas, B.: *J. Alloys Compd.* **479**, 49–55 (2009)
24. Joshi, G.K., Khot, A.Y., Sawant, S.R.: *Solid State Commun.* **65**(12), 1593–1595 (1988)
25. Pankhurst, Q.A., Pollard, R.J.: *Phys. Rev. Lett.* **67**, 248 (1991)
26. Duquea, J.G.S., Souzaa, E.A., Menesesa, C.T., Kubota, L.: *J. Phys. B, At. Mol. Phys.* **398**, 287–290 (2007)
27. Mansour, S.F.: *J. Magn. Magn. Mater.* **323**, 1735–1740 (2011)
28. Singh, N., Agarwal, A., Sanghi, S.: *Curr. Appl. Phys.* **11**, 783–789 (2011)
29. Jiang, J.Z., Goya, G.F., Rechenberg, H.R.: *J. Phys., Condens. Matter* **11**, 4063–4078 (1999)
30. Klinger, M.I.: *J. Phys. C, Solid State Phys.* **8**, 3595–3607 (1975)
31. Rana, M.U., Islam, M.U., Ishtiaq, A., Abbas, T.: *J. Magn. Magn. Mater.* **187**, 242 (1998)
32. Rana, M.U., Islam, M., Abbas, T.: *Solid State Commun.* **126**, 129–133 (2003)